PHYSICAL REVIEW LETTERS **131,** 076702 (2023)

Isotropic Spin Hall Effect in an Epitaxial Ferromagnet

Nozomi Soya,[1] Michihiro Yamada,[2,3] Kohei Hamaya,[2,4] and Kazuya Ando[1,5,6,*]
[1]*Department of Applied Physics and Physico-Informatics, Keio University, Yokohama 223-8522, Japan*
[2]*Center for Spintronics Research Network, Osaka University, 1-3 Machikaneyama, Toyonaka 560-8531, Japan*
[3]*PRESTO, Japan Science and Technology Agency, 4-1-8 Honcho, Kawaguchi, Saitama 332-0012, Japan*
[4]*Spintronics Research Network Division, Institute for Open and Transdisciplinary Research Initiatives, Osaka University, Yamadaoka 2-1, Suita, Osaka 565-0871, Japan*
[5]*Keio Institute of Pure and Applied Sciences, Keio University, Yokohama 223-8522, Japan*
[6]*Center for Spintronics Research Network, Keio University, Yokohama 223-8522, Japan*

(Received 16 January 2023; revised 2 May 2023; accepted 22 June 2023; published 17 August 2023)

We report the observation of the isotropic spin Hall effect in a ferromagnet. We show that the spin Hall effect in an epitaxially grown $\mathrm{Fe_3Si}$ generates a sizable spin current with a spin direction that is noncollinear with the magnetization. Furthermore, we find that the spin Hall current is independent of the relative orientation between its spin direction and the magnetization; the spin Hall effect is isotropic. This observation demonstrates that the intrinsically generated transverse spin component is protected from dephasing, providing fundamental insights into the generation and transport of spin currents in ferromagnets.

DOI: 10.1103/PhysRevLett.131.076702

Exploring the physics of spin transport in ferromagnetic metals (FMs) has been a central challenge in magnetism and spintronics. In a FM, an electric field $\mathbf{E}$ generates a spin-polarized current flowing along the $\mathbf{E}$ direction because majority and minority electrons with opposite spin directions exhibit different conductivities due to the exchange splitting [1]. In the presence of spin-orbit coupling, $\mathbf{E}$ also generates an anomalous Hall current flowing along the $\mathbf{m}\times\mathbf{E}$ direction, where $\mathbf{m}$ denotes the unit vector of the magnetization [2–5]. Since charge flow in FMs is spin polarized, the anomalous Hall current is accompanied by a spin current with a spin direction along $\mathbf{m}$, as shown in Fig. 1(a) [6–13]. The generation of such a spin current is referred to as the spin anomalous Hall effect (SAHE) [6]. In the SAHE, the spin direction $\boldsymbol{\sigma}$ of the spin current can be changed by controlling $\mathbf{m}$ because of $\boldsymbol{\sigma}\|\mathbf{m}$. This situation is contrary to the case of the spin Hall effect (SHE) in nonmagnetic metals (NMs), where $\boldsymbol{\sigma}$ is geometrically fixed; $\boldsymbol{\sigma}$ is perpendicular to both $\mathbf{E}$ and the flow direction of the spin current, as shown in Fig. 1(b) [14–18].

As in the case of the SAHE, it has been commonly assumed that the spin direction of spin currents in FMs is aligned with $\mathbf{m}$ because of spin dephasing, that is, misaligned spins rapidly precess in the exchange field and incoherent spin precession destroys the net spin density transverse to $\mathbf{m}$ [19]. However, recent theories have suggested that spin currents generated by the intrinsic mechanism of the SHE can have spin direction transverse to the magnetization, suggesting that the SHE with the conventional fixed geometry can exist even in FMs [see Fig. 1(c)]. In FMs, the spin Hall current is predicted to be the sum of a magnetization-independent isotropic spin Hall current and a magnetization-dependent anisotropic spin anomalous Hall current [8]. The prediction of this counterintuitive feature of intrinsically generated spin Hall currents has motivated experimental studies on the role of the magnetization in the conversion between charge and spin currents in FMs [20,21].

Despite the theoretical prediction and experimental efforts, the behavior of spin Hall currents in FMs remains controversial [8,20–32]; evidence for the magnetization-independent isotropic SHE is still lacking. Although magnetization angle dependence of the charge-spin conversion has been investigated experimentally, some studies have found that the charge-spin conversion is independent of the magnetization orientation [20,25], while others have found that the conversion depends on the magnetization [26,27] (see Supplemental Material [33]). One of the primary factors

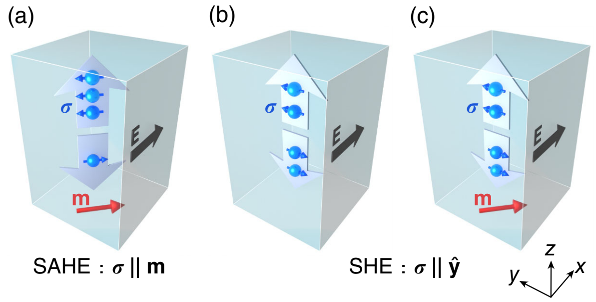

FIG. 1. Schematic illustrations of the (a) spin anomalous Hall effect, (b) spin Hall effect in a NM, and (c) spin Hall effect in a FM.

to these contradicting reports is the coexistence of the SHE and SAHE in these studies. For a comprehensive understanding of the spin Hall transport in FMs, quantifying the SHE free from the SAHE remains a major experimental challenge.

In this Letter, we provide experimental evidence of the magnetization-independent isotropic SHE in an epitaxial FM. The evidence is obtained by measuring current-induced spin-orbit torques (SOTs) for a Co/Ti/Fe_3Si trilayer, which is designed to detect the SHE free from the SAHE of the epitaxially grown Fe_3Si layer. We show that the SHE in the Fe_3Si layer is independent of the relative orientation between the spin direction of the spin Hall current and magnetization, demonstrating the unique property of the intrinsically generated spin current in the FM.

To clarify the intrinsic nature of spin Hall transport in a FM, we study the SOTs generated by epitaxially grown Fe_3Si, where the impact of disorders on the intrinsic SHE and spin transport is suppressed compared to polycrystalline systems. The SiO_2(4 nm)/Co(5 nm)/Ti (3 nm)/Fe_3Si(5 nm)/MgO(001)-substrate device was fabricated by molecular beam epitaxy and magnetron sputtering, where the numbers in parentheses represent the thickness [see Fig. 2(a)]. The 5-nm-thick Fe_3Si layer with cubic symmetry was grown on the MgO(001) substrate by molecular beam epitaxy at a growth temperature below 80 °C. Figure 2(b) shows the reflection high-energy electron diffraction (RHEED) pattern for the surface of the Fe_3Si layer. The results clearly exhibit the symmetrical streak, indicating good epitaxial growth of the Fe_3Si layer. Here, epitaxially grown Fe_3Si films are known to exhibit soft magnetic properties and small magnetic damping [39], which are prerequisites for characterizing the SHE in the trilayer structure (see also Supplemental Material [33]). From this perspective, we chose epitaxial Fe_3Si as a source of spin Hall currents over other epitaxial FMs such as Fe and Co with hard magnetic properties [40–43], or Ni with large magnetic damping [17]. In Fig. 2(c), we show the magnetization curve under in-plane magnetic field H for a SiO_2(4 nm)/Fe_3Si(5 nm)/MgO(001)-substrate film, where H was applied along the hard axis of the Fe_3Si layer ($\mathbf{H}\|[110]$). Figure 2(c) shows that the coercive field of the Fe_3Si layer is less than 5 mT, demonstrating its soft magnetic property. On the Fe_3Si layer, the SiO_2(4 nm)/Co(5 nm)/Ti(3 nm) layers were deposited by magnetron sputtering at room temperature. In the Co/Ti/Fe_3Si(001) device, the Co layer is magnetically separated from the Fe_3Si(001) layer by the Ti spacer.

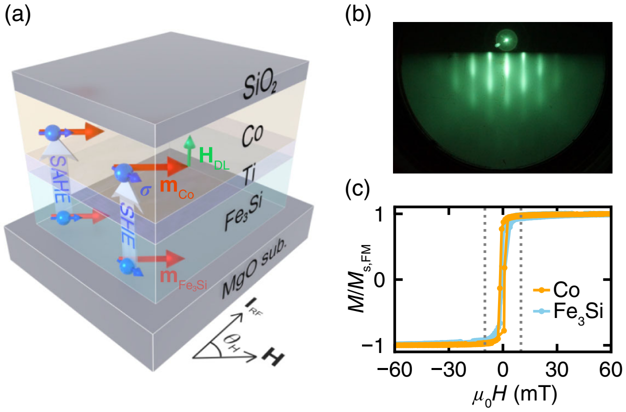

FIG. 2. (a) A schematic illustration of the Co/Ti/Fe_3Si(001) device and spin injection into the Co layer induced by the SAHE and SHE in the Fe_3Si layer. $\mathbf{H}_{\mathrm{DL}}$ denotes the dampinglike effective field. (b) The RHEED pattern from the surface of the Fe_3Si layer on the MgO(001) substrate. (c) The normalized magnetization curves under in-plane magnetic fields for SiO_2(4 nm)/Fe_3Si(001)(5 nm)/MgO(001)-substrate and SiO_2(4 nm)/Co(5 nm)/Ti(3 nm)/SiO_2-substrate films measured with a vibrating sample magnetometer. The dotted lines are ±10 mT.

The SOTs for the Co/Ti/Fe_3Si(001) device was measured using the spin-torque ferromagnetic resonance (ST-FMR). For the ST-FMR measurement, the Co/Ti/Fe_3Si(001) film was patterned into rectangular strips with a width of 10 μm and a length of 70 μm by using the photolithography and Ar-ion milling. A radio frequency (rf) current I_{rf} with a frequency of f was applied to the device along [010] direction of the Fe_3Si layer, and an in-plane external field H at an angle of θ_H was swept from −300 to 300 mT [see Fig. 2(a)]. The applied rf current generates a spin current by the SHE in the Fe_3Si layer. The spin current is injected into the Co layer through the Ti layer with sufficiently long spin diffusion length [44], exerting SOTs on the magnetization of the Co layer. The SOTs, including the dampinglike and fieldlike torques, as well as an Oersted field, induce magnetization precession in the Co layer at the FMR field of the Co layer, $H = H_{\mathrm{FMR,Co}}$. The magnetization precession yields resistance oscillations of the device due to the anisotropic magnetoresistance (AMR) of the Co layer. The change in the resistance mixes with the rf current to create a direct current (dc) voltage $V_{\mathrm{dc,Co}}$ across the bar at $H = H_{\mathrm{FMR,Co}}$ (see also Supplemental Material [33]). At the FMR field of the Fe_3Si layer, $H = H_{\mathrm{FMR,Fe_3Si}}$, the FMR of the Fe_3Si layer is driven by the SOTs and the Oersted field due to the current flow in the Co/Ti layer. The magnetization precession in the Fe_3Si layer produces dc voltage $V_{\mathrm{dc,Fe_3Si}}$ through the AMR of the Fe_3Si layer. We measured $V_{\mathrm{dc}} = V_{\mathrm{dc,Co}} + V_{\mathrm{dc,Fe_3Si}}$ using a bias tee at room temperature.

The ST-FMR for the Co/Ti/Fe_3Si(001) device allows us to extract the SHE from the mixture of the SHE and SAHE of the Fe_3Si layer. In the Fe_3Si layer, both SHE and SAHE generate spin currents. However, only the SHE can exert SOTs on the magnetization of the Co layer. The reason for this is that, owing to the soft magnetic properties of epitaxial Fe_3Si, the magnetization of the Co layer $\mathbf{m}_{\mathrm{Co}}$ and that of the Fe_3Si layer $\mathbf{m}_{\mathrm{Fe_3Si}}$ are aligned parallel at $H = H_{\mathrm{FMR,Co}}$: $\mathbf{m}_{\mathrm{Co}}\|\mathbf{m}_{\mathrm{Fe_3Si}}\|\mathbf{H}$ [see Fig. 2(c)]. In this situation, the spin polarization $\boldsymbol{\sigma}(\|\mathbf{m}_{\mathrm{Fe_3Si}})$ of spin currents

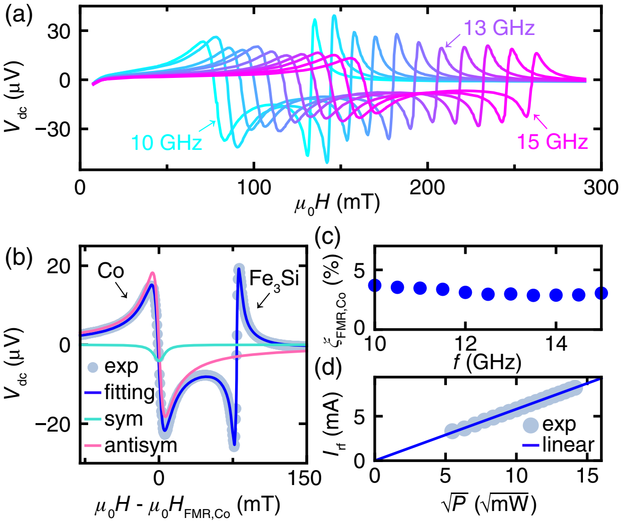

FIG. 3. (a) H dependence of V_{dc} for the Co/Ti/Fe$_3$Si(001) device at $\theta_H = 45°$. The rf frequency was varied from $f = 10$ to 15 GHz. (b) V_{dc} at $f = 13$ GHz. The spectrum consists of the FMR of the Co layer and that of the Fe$_3$Si layer, as indicated by the black arrows. The blue solid curve is the total fitting result using Eq. (1). The green(pink) curve is the symmetric(antisymmetric) component of $V_{dc,Co}$. (c) f dependence of $\xi_{FMR,Co}$. (d) I_{rf} as a function of the square root of P. The solid circles are the experimental data, and the solid line is the linear fit to the data.

generated by the SAHE in the Fe$_3$Si layer is parallel to $\mathbf{m}_{Co}$: $\boldsymbol{\sigma} \| \mathbf{m}_{Co}$ [see Fig. 2(a)]. Since the dampinglike torque is produced by the component of incident spins transverse to $\mathbf{m}_{Co}$, the SAHE in the Fe$_3$Si layer does not exert a dampinglike torque on $\mathbf{m}_{Co}$. In contrast, the SHE generates the dampinglike torque [see Fig. 2(a)], enabling us to investigate the SHE of the Fe$_3$Si layer free from the SAHE (see also Supplemental Material [33]).

Figure 3(a) shows the ST-FMR spectra for the Co/Ti/Fe$_3$Si(001) device measured at $\theta_H = 45°$. The ST-FMR spectra are composed of two signals due to the FMR of the Co and Fe$_3$Si layers, as shown in Fig. 3(b): $V_{dc} = V_{dc,Co} + V_{dc,Fe_3Si}$. The saturation magnetization of the Co ($\mu_0 M_{s,Co} = 1.36$ T) and Fe$_3$Si ($\mu_0 M_{s,Fe_3Si} = 1.08$ T) layers indicates that the signals with the smaller and larger resonance fields correspond to the FMR of the Co and Fe$_3$Si layers, respectively [45]. Each ST-FMR signal at $H = H_{FMR,Co}$ and $H = H_{FMR,Fe_3Si}$ consists of symmetric and antisymmetric components as [46]

$$\begin{aligned} V_{dc} &= V_{dc,Co} + V_{dc,Fe_3Si} \\ &= \sum_{FM=Co,Fe_3Si} \left\{ S_{FM} \frac{W_{FM}^2}{(\mu_0 H - \mu_0 H_{FMR,FM})^2 + W_{FM}^2} \right. \\ &\quad \left. + A_{FM} \frac{W_{FM}(\mu_0 H - \mu_0 H_{FMR,FM})}{(\mu_0 H - \mu_0 H_{FMR,FM})^2 + W_{FM}^2} \right\}, \end{aligned} \tag{1}$$

where $H_{FMR,FM}$ is the resonance field of the FM layer and W_{FM} is the spectral width, where FM = Co, Fe$_3$Si. The symmetric component S_{FM} arises from an out-of-plane field due to the dampinglike effective field, and the antisymmetric component A_{FM} arises from an in-plane field due to the Oersted field and fieldlike effective field. We fitted the measured V_{dc} signals using Eq. (1) as shown in Fig. 3(b) (see the blue solid curve). From the fitting result, we find that the FMR spin-torque generation efficiency $\xi_{FMR,Co}$ is independent of f, as shown in Fig. 3(c), which supports the validity of the ST-FMR measurement [47] (for details, see Supplemental Material [33]).

To investigate the SHE in the Fe$_3$Si layer, we characterize $V_{dc,Co}$ at $H = H_{FMR,Co}$, where the magnetization of the Co layer detects the SOTs generated by the SHE in the Fe$_3$Si layer. From the ST-FMR signal $V_{dc,Co}$, we determine the dampinglike torque efficiency per applied electric field E,

$$\xi_{DL,Co}^E = \frac{2e}{\hbar} \frac{\mu_0 M_{s,Co} d_{Co} H_{DL}}{E}, \tag{2}$$

which corresponds to the effective spin Hall conductivity [48]. Here, the dampinglike effective field H_{DL} acting on the magnetization of the Co layer can be quantified from the values of S_{Co}, obtained by fitting the measured V_{dc} signals, using [49,50]

$$\begin{aligned} S_{Co} &= \frac{I_{rf} \Delta R}{2\sqrt{2}} \mu_0 H_{DL} \\ &\quad \times \frac{\sqrt{\mu_0 H_{FMR,Co}(\mu_0 H_{FMR,Co} + \mu_0 M_{eff,Co})}}{W_{Co}(2\mu_0 H_{FMR,Co} + \mu_0 M_{eff,Co})}, \end{aligned} \tag{3}$$

where I_{rf} is the rf current flowing in the ST-FMR device and ΔR is the resistance change of the ST-FMR device due to the AMR in the Co layer. The contribution from the Fe$_3$Si layer to ΔR was carefully subtracted by measuring the AMR of a SiO$_2$(4 nm)/Fe$_3$Si(5 nm)/MgO-substrate reference device. We determined I_{rf} by measuring the resistance change of the device due to the Joule heating induced by currents [49]. Figure 3(d) shows the relation between the rf power P and rf current I_{rf} determined by comparing the resistance change due to the dc and rf current applications. Using the estimated rf current and measured device resistance, we obtain $\xi_{DL,Co}^E = 400\ \Omega^{-1}\ \text{cm}^{-1}$ for the dampinglike torque acting on the magnetization of the Co layer. From A_{Co}, we also obtain the fieldlike torque efficiency as $\xi_{FL,Co}^E = 386\ \Omega^{-1}\ \text{cm}^{-1}$ (see Supplemental Material [33]).

The obtained value of $\xi_{DL,Co}^E$ is dominated by the SHE in the Fe$_3$Si layer. In the Co/Ti/Fe$_3$Si(001) device, the SHE in the Ti layer and interfacial effects from the Co/Ti and Ti/Fe$_3$Si interfaces can also contribute to $\xi_{DL,Co}^E$. We assume that the contribution from the SHE in the Ti layer to $\xi_{DL,Co}^E$ is negligible because the spin Hall conductivity of Ti is vanishingly small compared to the measured value of

$\xi^{E}_{\mathrm{DL,Co}}$ [44]. We also assume that the orbital torque plays a minor role due to the fact that it is primarily pronounced in devices with thick Ti and FM layers and that Co is relatively insensitive to orbital injection [51,52]. This assumption is supported by the fact that the measured value of $\xi^{E}_{\mathrm{DL,Co}}$ is larger than the orbital torque efficiency of a Ni(8 nm)/Ti(3 nm) film, where the orbital response is pronounced due to the strong spin-orbit correlation in Ni [51]. To estimate the contribution from the Ti/$\mathrm{Fe_3Si}$ interface to $\xi^{E}_{\mathrm{DL,Co}}$, we measured the ST-FMR for a $\mathrm{SiO_2}$(4 nm)/Ti(3 nm)/$\mathrm{Fe_3Si}$(5 nm)(001)/MgO(001)-substrate reference device. In this device, the $\mathrm{Fe_3Si}$ layer is a detection layer of the SOTs. For the Ti/$\mathrm{Fe_3Si}$(001) device, we obtain $\xi^{E}_{\mathrm{DL,Fe_3Si}} = -30.6\ \Omega^{-1}\,\mathrm{cm}^{-1}$, which is more than an order of magnitude smaller than $\xi^{E}_{\mathrm{DL,Co}}$ for the Co/Ti/$\mathrm{Fe_3Si}$(001) device. This result suggests that the Ti/$\mathrm{Fe_3Si}$ interface plays a minor role in generating the SOTs. We have also estimated $\xi^{E}_{\mathrm{DL,Fe_3Si}}$ for the Co/Ti/$\mathrm{Fe_3Si}$(001) device from the ST-FMR signal of the $\mathrm{Fe_3Si}$ layer. Here, the FMR of the $\mathrm{Fe_3Si}$ layer is not only driven by the Oersted field, but also by the SOTs that can be generated by the Co/Ti interface, the Ti/$\mathrm{Fe_3Si}$ interface, and the bulk of the Co layer. From the measured value of $V_{\mathrm{dc,Fe_3Si}}$ [see Fig. 3(b)], we obtain $\xi^{E}_{\mathrm{DL,Fe_3Si}} = -37.3\ \Omega^{-1}\,\mathrm{cm}^{-1}$, which is more than an order of magnitude smaller than $\xi^{E}_{\mathrm{DL,Co}}$ for the Co/Ti/$\mathrm{Fe_3Si}$(001) device. The small difference in $\xi^{E}_{\mathrm{DL,Fe_3Si}}$ between the Ti/$\mathrm{Fe_3Si}$(001) and Co/Ti/$\mathrm{Fe_3Si}$(001) devices suggests that the dampinglike torque originating from the Co/Ti interface and the Co layer are negligible. Since the magnitude and sign of the SHE in Co depend on the current orientation with respect to the crystallographic axes [8], the SHE in polycrystalline Co is nontrivial. Our result suggests that the sign of the SHE in the sputtered Co layer is negative. This result is consistent with a recent experimental study [53]. Here, the small dampinglike torque acting on the $\mathrm{Fe_3Si}$ magnetization in the Co/Ti/$\mathrm{Fe_3Si}$(001) film shows that the FMR of the $\mathrm{Fe_3Si}$ layer is primarily driven by the Oersted field, which is consistent with the fact that $V_{\mathrm{dc,Fe_3Si}}$ is dominated by the antisymmetric component [see Fig. 3(b)].

Since the dampinglike torque arises from the component of injected spins transverse to the magnetization, the observation of the dampinglike torque on $\mathbf{m}_{\mathrm{Co}}$ demonstrates that the SHE in the $\mathrm{Fe_3Si}$ layer generates a substantial spin Hall current whose spin direction is noncollinear with $\mathbf{m}_{\mathrm{Fe_3Si}}$ because $\mathbf{m}_{\mathrm{Fe_3Si}} \| \mathbf{m}_{\mathrm{Co}}$. The transport of spins misaligned with the magnetization is counterintuitive because transverse spins are expected to precess and quickly dephase in a FM due to the strong exchange field. In fact, when electrons with spins transverse to the magnetization are injected into a FM, the net transverse spin density rapidly vanishes [19,54–57]. In this situation, the transmitted state is a superposition of majority and minority eigenstates with the same energy at different wave vectors due to the exchange splitting. Because of the different wave vectors, the phase difference between the majority and minority eigenstates varies in space, resulting in the oscillation of spins about the magnetization. The spin precession is incoherent among the injected electrons, leading to dephasing. In contrast, spin currents generated by the intrinsic mechanism of the SHE in a FM are predicted to be protected from dephasing despite the exchange splitting [8,19]. In the intrinsic SHE, an applied electric field couples eigenstates with different energies at the same wave vector. Since the perturbed state has only a single wave vector, the spin direction does not exhibit spatial oscillations, and thus a transverse component of the spin direction can exist in the FM.

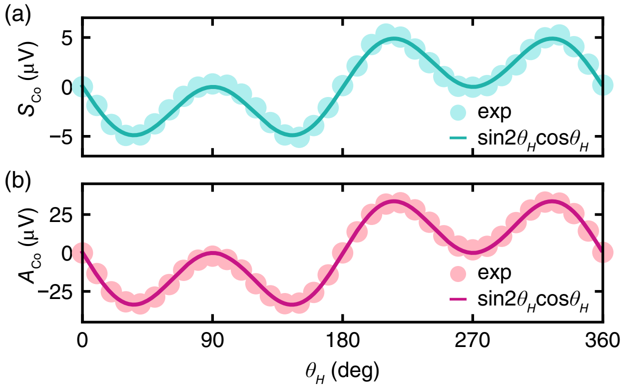

FIG. 4. θ_H dependence of (a) S_{Co} and (b) A_{Co} at $f = 13$ GHz for the Co/Ti/$\mathrm{Fe_3Si}$(001) device. The solid circles are the experimental data, and the solid curve is the fitting result using a function proportional to $\sin 2\theta_H \cos\theta_H$.

To investigate the spin Hall transport with a spin direction $\boldsymbol{\sigma}$ that is noncollinear with $\mathbf{m}_{\mathrm{Fe_3Si}}$, we change the relative orientation between $\boldsymbol{\sigma}$ and $\mathbf{m}_{\mathrm{Fe_3Si}}$ by rotating $\mathbf{m}_{\mathrm{Fe_3Si}}$ [see Fig. 2(a)]. In Fig. 4, we show θ_H dependence of S_{Co} and A_{Co} for the Co/Ti/$\mathrm{Fe_3Si}$(001) device. Here, the in-plane angle of $\mathbf{m}_{\mathrm{Fe_3Si}}$ is $\theta_{\mathrm{Fe_3Si}} = \theta_H$ because $\mathbf{m}_{\mathrm{Fe_3Si}}$ is aligned along H at the FMR field. Figure 4 shows $S_{\mathrm{Co}} \propto \sin 2\theta_H \cos\theta_H$ and $A_{\mathrm{Co}} \propto \sin 2\theta_H \cos\theta_H$. In the following, we focus on S_{Co}, which is proportional to an out-of-plane effective field h_z due to the dampinglike torque, dominated by the SHE in the $\mathrm{Fe_3Si}$ layer as discussed above.

We consider a situation where the SHE generates a spin Hall current Q_z^y flowing in the $\hat{\mathbf{z}}$ direction with a spin direction $\boldsymbol{\sigma}$ along the $\hat{\mathbf{y}}$ direction by an application of $\mathbf{E}$ along the $\hat{\mathbf{x}}$ direction. The injection of Q_z^y into a FM layer exerts an out-of-plane effective field, which is expressed as $h_z = H_{\mathrm{DL}}|\mathbf{m}\times\boldsymbol{\sigma}| = H_{\mathrm{DL}}\cos\theta_{\mathrm{FM}} = H_{\mathrm{DL}}\cos\theta_H$, where $\mathbf{m}$ is assumed to be aligned with the external magnetic field, and θ_{FM} is the magnetization angle. The dampinglike effective field H_{DL} is proportional to Q_z^y injected into the FM layer, and thus $h_z \propto Q_z^y \cos\theta_H$. Since S is proportional to h_z, we obtain $S \propto Q_z^y \sin 2\theta_H \cos\theta_H$, where the $\sin 2\theta_H$ component arises from the AMR in the FM detecting layer (for details, see Supplemental Material [33]).

The θ_H dependence of S_{Co} shown in Fig. 4(a) provides evidence that the SHE in the $\mathrm{Fe_3Si}$ layer is isotropic. In the relation $S_{\mathrm{Co}} \propto Q_z^y \sin 2\theta_H \cos\theta_H$ for the $\mathrm{Co/Ti/Fe_3Si(001)}$ device, the θ_H dependence of Q_z^y is nontrivial. The reason for this is that, in the $\mathrm{Fe_3Si}$ layer, the change in θ_H changes the relative angle between the spin direction $\boldsymbol{\sigma}$ of the spin Hall current and $\mathbf{m}_{\mathrm{Fe_3Si}}$, such as transverse spin transport ($\boldsymbol{\sigma}\perp\mathbf{m}_{\mathrm{Fe_3Si}}$) at $\theta_H = 0$ and longitudinal spin transport ($\boldsymbol{\sigma}\|\mathbf{m}_{\mathrm{Fe_3Si}}$) at $\theta_H = 90°$. If the spin Hall current Q_z^y depends on the relative angle between $\boldsymbol{\sigma}$ and $\mathbf{m}_{\mathrm{Fe_3Si}}$, i.e., the SHE in the $\mathrm{Fe_3Si}$ layer is anisotropic, S_{Co} cannot be proportional to $\sin 2\theta_H \cos\theta_H$ because Q_z^y changes with θ_H. Nevertheless, we find $S_{\mathrm{Co}} \propto \sin 2\theta_H \cos\theta_H$, indicating that Q_z^y due to the SHE in the $\mathrm{Fe_3Si}$ layer is independent of θ_H. This result shows that the spin Hall current generated in the $\mathrm{Fe_3Si}$ layer is independent of the magnetization orientation, providing experimental evidence that the intrinsic spin Hall current is free from spin dephasing and SHE is isotropic with respect to the magnetization. This result is also supported by $A_{\mathrm{Co}} \propto \sin 2\theta_H \cos\theta_H$ shown in Fig. 4(b), which is consistent with the isotropic SHE (for details, see Supplemental Material [33]). The observation of the isotropic SHE in $\mathrm{Fe_3Si}$ is consistent with recent first-principles calculations on cubic FMs [8]. Here, the $\sin 2\theta_H \cos\theta_H$ dependence of S_{Co} and A_{Co} also indicates the absence of unconventional spin currents, such as Q_z^x, due to the additional symmetry breaking by the magnetization in the $\mathrm{Co/Ti/Fe_3Si(001)}$ device [21,30,58].

In summary, we have demonstrated the isotropic SHE in the epitaxial ferromagnet by measuring the SOTs for the $\mathrm{Co/Ti/Fe_3Si(001)}$ device. From the ST-FMR, we found that the SHE in the $\mathrm{Fe_3Si}$ layer generates spin Hall currents with a spin direction $\boldsymbol{\sigma}$ non-collinear with the magnetization $\mathbf{m}_{\mathrm{Fe_3Si}}$. Furthermore, we found that the spin Hall current in the $\mathrm{Fe_3Si}$ layer is unchanged by the change in the direction of $\mathbf{m}_{\mathrm{Fe_3Si}}$. This result demonstrates that the intrinsically generated transverse spins are free from dephasing and that the SHE in the ferromagnet is isotropic. The isotropic SHE highlights the fundamental difference between intrinsically generated and externally injected spin currents, which deepen our understanding of the spin transport in FMs.

This work was supported by JSPS KAKENHI (Grants No. 22H04964, No. 20H00337, No. 20H02593, No. 19H05616), Spintronics Research Network of Japan (Spin-RNJ), and MEXT Initiative to Establish Next-generation Novel Integrated Circuits Centers (X-NICS) (Grant No. JPJ011438). N. S. is supported by JSPS Grant-in-Aid for Research Fellowship for Young Scientists (DC1) (Grant No. 22KJ2714). M. Y. is supported by JST PRESTO (Grant No. JPMJPR20BA).

*ando@appi.keio.ac.jp

[1] J. Slonczewski, J. Magn. Magn. Mater. **159**, L1 (1996).
[2] E. M. Pugh and N. Rostoker, Rev. Mod. Phys. **25**, 151 (1953).
[3] R. Karplus and J. M. Luttinger, Phys. Rev. **95**, 1154 (1954).
[4] N. Nagaosa, J. Sinova, S. Onoda, A. H. MacDonald, and N. P. Ong, Rev. Mod. Phys. **82**, 1539 (2010).
[5] Y. Omori, E. Sagasta, Y. Niimi, M. Gradhand, L. E. Hueso, F. Casanova, and Y. C. Otani, Phys. Rev. B **99**, 014403 (2019).
[6] T. Taniguchi, J. Grollier, and M. D. Stiles, Phys. Rev. Appl. **3**, 044001 (2015).
[7] T. Y. Ma, C. H. Wan, X. Wang, W. L. Yang, C. Y. Guo, C. Fang, M. K. Zhao, J. Dong, Y. Zhang, and X. F. Han, Phys. Rev. B **101**, 134417 (2020).
[8] V. P. Amin, J. Li, M. D. Stiles, and P. M. Haney, Phys. Rev. B **99**, 220405(R) (2019).
[9] S. Iihama, T. Taniguchi, K. Yakushiji, A. Fukushima, Y. Shiota, S. Tsunegi, R. Hiramatsu, S. Yuasa, Y. Suzuki, and H. Kubota, Nat. Electron. **1**, 120 (2018).
[10] Y. Miura and K. Masuda, Phys. Rev. Mater. **5**, L101402 (2021).
[11] T. Seki, S. Iihama, T. Taniguchi, and K. Takanashi, Phys. Rev. B **100**, 144427 (2019).
[12] J. D. Gibbons, D. MacNeill, R. A. Buhrman, and D. C. Ralph, Phys. Rev. Appl. **9**, 064033 (2018).
[13] C. Qin, S. Chen, Y. Cai, F. Kandaz, and Y. Ji, Phys. Rev. B **96**, 134418 (2017).
[14] J. E. Hirsch, Phys. Rev. Lett. **83**, 1834 (1999).
[15] Y. K. Kato, R. C. Myers, A. C. Gossard, and D. D. Awschalom, Science **306**, 1910 (2004).
[16] N. Soya, H. Hayashi, T. Harumoto, T. Gao, S. Haku, and K. Ando, Phys. Rev. B **103**, 174427 (2021).
[17] H. Hayashi, A. Musha, H. Sakimura, and K. Ando, Phys. Rev. Res. **3**, 013042 (2021).
[18] S. Haku, H. Moriya, H. An, A. Musha, and K. Ando, Phys. Rev. B **104**, 174403 (2021).
[19] A. Davidson, V. P. Amin, W. S. Aljuaid, P. M. Haney, and X. Fan, Phys. Lett. A **384**, 126228 (2020).
[20] M. Cosset-Chéneau, M. H. Fahmy, A. Kandazoglou, C. Grezes, A. Brenac, S. Teresi, P. Sgarro, P. Warin, A. Marty, V. T. Pham, J.-P. Attané, and L. Vila, Phys. Rev. B **106**, L220405 (2022).
[21] W. L. Yang, J. W. Wei, C. H. Wan, Y. W. Xing, Z. R. Yan, X. Wang, C. Fang, C. Y. Guo, G. Q. Yu, and X. F. Han, Phys. Rev. B **101**, 064412 (2020).
[22] G. Qu, K. Nakamura, and M. Hayashi, Phys. Rev. B **102**, 144440 (2020).
[23] F. Freimuth, S. Blügel, and Y. Mokrousov, Phys. Rev. Lett. **105**, 246602 (2010).
[24] C. O. Pauyac, M. Chshiev, A. Manchon, and S. A. Nikolaev, Phys. Rev. Lett. **120**, 176802 (2018).
[25] D. Tian, Y. Li, D. Qu, S. Y. Huang, X. Jin, and C. L. Chien, Phys. Rev. B **94**, 020403(R) (2016).
[26] J. Cramer, A. Ross, S. Jaiswal, L. Baldrati, R. Lebrun, and M. Kläui, Phys. Rev. B **99**, 104414 (2019).
[27] K. S. Das, W. Y. Schoemaker, B. J. van Wees, and I. J. Vera-Marun, Phys. Rev. B **96**, 220408(R) (2017).
[28] Q. Fu, L. Liang, W. Wang, L. Yang, K. Zhou, Z. Li, C. Yan, L. Li, H. Li, and R. Liu, Phys. Rev. B **105**, 224417 (2022).

[29] W. Wang, Z. Yan, Y. Cao, C. Gao, Z. Shi, M. Si, J. Cao, L. Xi, D. Yang, and D. Xue, Adv. Funct. Mater. **32**, 2204212 (2022).

[30] A. M. Humphries, T. Wang, E. R. Edwards, S. R. Allen, J. M. Shaw, H. T. Nembach, J. Q. Xiao, T. J. Silva, and X. Fan, Nat. Commun. **8**, 1 (2017).

[31] W. Wang, T. Wang, V. P. Amin, Y. Wang, A. Radhakrishnan, A. Davidson, S. R. Allen, T. J. Silva, H. Ohldag, D. Balzar *et al.*, Nat. Nanotechnol. **14**, 819 (2019).

[32] B. F. Miao, S. Y. Huang, D. Qu, and C. L. Chien, Phys. Rev. Lett. **111**, 066602 (2013).

[33] See Supplemental Material at http://link.aps.org/supplemental/10.1103/PhysRevLett.131.076702 for the detailed descriptions of the comparison with previous works, rectification effect due to the giant magnetoresistance, spin-orbit torque due to the spin anomalous Hall effect in Fe_3Si, and model of the spin-torque ferromagnetic resonance, which includes Refs. [34–38].

[34] E. Tsymbal and D. Pettifor, *Perspectives of Giant Magnetoresistance*, edited by H. Ehrenreich and F. Spaepen, Solid State Physics Vol. 56 (Academic Press, New York, 2001), pp. 113–237.

[35] O. Mosendz, V. Vlaminck, J. E. Pearson, F. Y. Fradin, G. E. W. Bauer, S. D. Bader, and A. Hoffmann, Phys. Rev. B **82**, 214403 (2010).

[36] T. McGuire and R. Potter, IEEE Trans. Magn. **11**, 1018 (1975).

[37] J. Sklenar, W. Zhang, M. B. Jungfleisch, W. Jiang, H. Saglam, J. E. Pearson, J. B. Ketterson, and A. Hoffmann, J. Appl. Phys. **120** (2016).

[38] Y. Kageyama, Y. Tazaki, H. An, T. Harumoto, T. Gao, J. Shi, and K. Ando, Sci. Adv. **5**, eaax4278 (2019).

[39] S. Oki, Y. Sasaki, Y. Kasatani, S. Yamada, S. Mizukami, Y. Nozaki, and K. Hamaya, J. Condens. Matter Phys. **30**, 255802 (2018).

[40] K. B. Hathaway and G. A. Prinz, Phys. Rev. Lett. **47**, 1761 (1981).

[41] M. Gester, C. Daboo, R. Hicken, S. Gray, A. Ercole, and J. C. Bland, J. Appl. Phys. **80**, 347 (1996).

[42] G. A. Prinz, Phys. Rev. Lett. **54**, 1051 (1985).

[43] Y. Nukaga, M. Ohtake, M. Futamoto, F. Kirino, N. Fujita, and N. Inaba, IEEE Trans. Magn. **45**, 2519 (2009).

[44] C. Du, H. Wang, F. Yang, and P. C. Hammel, Phys. Rev. B **90**, 140407(R) (2014).

[45] C. Kittel, Phys. Rev. **73**, 155 (1948).

[46] L. Liu, T. Moriyama, D. C. Ralph, and R. A. Buhrman, Phys. Rev. Lett. **106**, 036601 (2011).

[47] W. Zhang, W. Han, X. Jiang, S.-H. Yang, and S. S. P. Parkin, Nat. Phys. **11**, 496 (2015).

[48] M.-H. Nguyen, D. C. Ralph, and R. A. Buhrman, Phys. Rev. Lett. **116**, 126601 (2016).

[49] V. Tshitoyan, C. Ciccarelli, A. P. Mihai, M. Ali, A. C. Irvine, T. A. Moore, T. Jungwirth, and A. J. Ferguson, Phys. Rev. B **92**, 214406 (2015).

[50] D. Fang, H. Kurebayashi, J. Wunderlich, K. Výborný, L. P. Zârbo, R. Campion, A. Casiraghi, B. Gallagher, T. Jungwirth, and A. Ferguson, Nat. Nanotechnol. **6**, 413 (2011).

[51] H. Hayashi, D. Jo, D. Go, T. Gao, S. Haku, Y. Mokrousov, H.-W. Lee, and K. Ando, Commun. Phys. **6**, 32 (2023).

[52] D. Lee, D. Go, H.-J. Park, W. Jeong, H.-W. Ko, D. Yun, D. Jo, S. Lee, G. Go, J. H. Oh, K.-J. Kim, B.-G. Park, B.-C. Min, H. C. Koo, H.-W. Lee, O. Lee, and K.-J. Lee, Nat. Commun. **12**, 6710 (2021).

[53] T.-Y. Chen, Y.-C. Hsiao, W.-B. Liao, and C.-F. Pai, Phys. Rev. Appl. **17**, 064005 (2022).

[54] A. Ghosh, S. Auffret, U. Ebels, and W. E. Bailey, Phys. Rev. Lett. **109**, 127202 (2012).

[55] M. D. Stiles and A. Zangwill, Phys. Rev. B **66**, 014407 (2002).

[56] M. Zwierzycki, Y. Tserkovnyak, P. J. Kelly, A. Brataas, and G. E. W. Bauer, Phys. Rev. B **71**, 064420 (2005).

[57] D. Ralph and M. Stiles, J. Magn. Magn. Mater. **320**, 1190 (2008).

[58] Y. Hibino, T. Taniguchi, K. Yakushiji, A. Fukushima, H. Kubota, and S. Yuasa, Nat. Commun. **12**, 6254 (2021).